Chapter 6
Titanium Alloys: Part 2—Alloy Development, Properties and Applications

A. Bhattacharjee, B. Saha and J.C. Williams

Abstract Titanium alloys are the principal replacements, and in many cases also prime candidate materials to replace (i) aerospace special and advanced steels, owing to their significantly higher usable specific strength properties, (ii) aluminium alloys due to their better elevated temperature properties and (iii) nickel-base superalloys for much of the high pressure compressors (HPCs) of modern engines, owing to their superior medium temperature (up to 550 °C) creep strength and acceptable oxidation and corrosion resistances. This chapter summarizes the chemical compositions, properties and applications of commercially pure α-titanium, near-α, α + β and β titanium alloys.

Keywords Titanium alloys · Secondary processing · Microstructures · Mechanical properties · Fatigue · Fracture · Applications

6.1 Introduction

Conventional titanium alloys consisting of α-titanium, near-α, α + β and β titanium alloys are used in various engineering sectors, but predominantly for aerospace because of cost. These alloys possess good corrosion resistance and a range of strengths starting from commercially pure titanium up to the high strength β titanium alloys, which can compete with steels on a density normalized basis. The near-α titanium alloys have the best combinations of strength and high temperature

A. Bhattacharjee (✉)
Materials Processing Division, DMRL, Hyderabad, India
e-mail: amitb@dmrl.drdo.in

B. Saha
RCMA (Materials), CEMILAC, Hyderabad, India
e-mail: bsaha@cemilac.drdo.in

J.C. Williams
Dept. of Materials Science & Engineering, The Ohio State University, Columbus, USA
e-mail: williams.1726@osu.edu

N. Eswara Prasad and R.J.H. Wanhill (eds.), *Aerospace Materials and Material Technologies*, Indian Institute of Metals Series,
DOI 10.1007/978-981-10-2134-3_6

properties and are the natural choice for high temperature aerospace applications. The α + β titanium alloys have good strength and medium temperature capability.

In this chapter a review of each of these classes of titanium alloys will be given, and their generic processing, microstructure, mechanical properties and applications will be concisely discussed. The reader may obtain more details from the Bibliography.

6.2 Titanium Alloy Developments and Applications

There are numerous review articles and monographs that cover titanium alloy development as well as their production and applications aspects in detail [1–40]. In this section these aspects are dealt with briefly.

6.2.1 Commercially Pure Titanium and α-Titanium Alloys

All α-titanium alloys are based on the low temperature, hexagonal allotropic form of titanium. These alloys can contain substitutional alloying elements (Al or Sn) or interstitial elements (oxygen, carbon or nitrogen) that are soluble in the hexagonal α phase. These alloys also contain limited quantities of elements with limited solubility, such as Fe, V and Mo.

Specific alloys have been formulated to improve the environmental resistance of CP titanium and α-titanium alloys to provide comparable performance at reduced cost. Table 6.1 lists these alloys, their compositions and typical yield strengths.

All the alloys derive their characteristics from the hexagonal α phase, as mentioned earlier. The strengthening and processing aspects of these alloys can be obtained from Refs. [1, 25] and are summarized in Table 6.2 and Fig. 6.1, respectively. Referring to Fig. 6.1, stage II processing controls the preferred orientation (texture) intensity and α grain size; and the microstructure after stage III processing is controlled by the degree of deformation and the annealing temperature, which influences the α grain size with marginal effect on texture intensity.

Applications The excellent corrosion resistance of CP titanium, its good weldability and general fabricability have resulted in its use for aerospace tubing, e.g. in anti-icing ducts. However, the alloys Ti-2.5Cu and Ti-3-Al-2.5V offer higher strength alternatives with similar ease of fabrication (Ti-2.5 Cu in the annealed condition). Also, Ti-25Cu in the aged condition is used in engine bypass ducts owing to a higher temperature capability (up to 350 °C).

Table 6.1 Compositions and 0.2 % yield strengths of commercial CP titanium and α-titanium alloys [1]

Alloy		O (max) wt%	Fe (max) wt%	Other elements	0.2 % Yield strength (MPa)
CP titanium					
CP	Grade 1 Grade 2 Grade 3 Grade 4	0.18 0.25 0.35 0.40	0.20 0.30 0.30 0.50		170 275 380 480
Ti–0.2Pd	Grade 7 Grade 11	0.25 0.18	0.30 0.20	0.12–0.25Pd	275 170
Ti–0.05Pd	Grade 16 Grade 17	0.25 0.18	0.30 0.20	0.04–0.08Pd	275 170
Ti–0.1Ru	Grade 26 Grade 27	0.25 0.18	0.30 0.20	0.08–0.14Ru	275 170
α-titanium alloys					
Ti–0.3Mo–0.9Ni (Grade 12)		0.25	0.25	0.2–0.4Mo, 0.6–0.9Ni	345
Ti–2.5Cu		0.20	0.20	2.5Cu	600
Ti–3Al–2.5V (Grade 9)		0.15	0.25	2.5–3.5Al, 2.0–3.0V	485
Ti–3Al–2.5V–0.05Pd (Grade 18)		0.15	0.25	2.5–3.5Al, 2.0–3.0V, (+Pd)	485
Ti–3Al–2.5V–0.1Ru (Grade 28)		0.25	0.25	2.5–3.5Al, 2.0–3.0V, (+Ru)	485
Ti–5Al–2.5Sn (Grade 6)		0.20	0.20	4.0–6.0Al, 2.0–3.0Sn	795
Ti–5Al–2.5Sn ELI		0.15	0.25	4.75–5.75Al, 2.0–3.0Sn	725

Table 6.2 Strengthening mechanisms in CP titanium and α-titanium alloys [1]

Strengthening mechanism	Dependence	Examples/limitations
Grain size	$d^{-1/2}$	Fine grains limit twinning
Interstitial solid solution	$c^{1/2}$	Strain localization >2500 ppm oxygen
Substitutional solid solution	c	Strain localization >5 % Al equivalence
Texture	c-axis orientation	Max. strength when loaded along c-axis
Precipitation	$r^{1/2}$, $f^{1/2}$	Ti–2.5Cu; other alloys >5.5 % Al equivalence

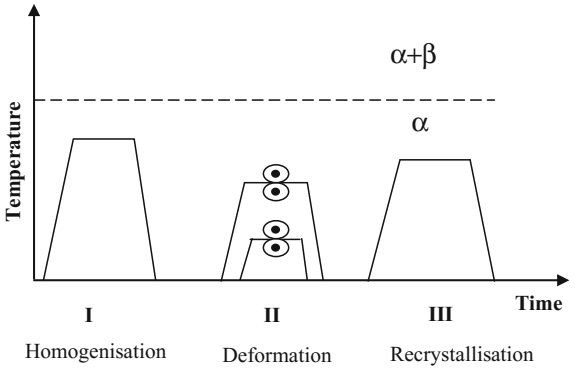

Fig. 6.1 Schematic of processing for CP titanium and α-titanium alloys [1]

6.2.2 *High Temperature Near-α Titanium Alloys*

Alloy development For long-term applications at high temperatures the α + β titanium alloys, such as Ti–6Al–4V, are limited to about 350 °C. For higher temperatures near-α alloys such as Ti–6Al–2Sn–4Zr–2Mo + Si (Ti–6242) and Ti–5.8Al–4Sn–3.5Zr–0.5Mo–0.7Nb–0.35Si–0.06C (IMI 834) have been developed according to the following general principles:

(1) The diffusion rates in the β phase are about two orders of magnitude faster than in the α phase. Therefore the volume fraction of β phase is reduced in these high temperature alloys as compared to Ti–6Al–4V.
(2) The decrease in volume fraction of β phase in Ti–6242 and IMI 834 is achieved by reducing the total content of β stabilizing elements and by alloying with the α stabilizers Sn and Zr as well as about 6 wt% Al.
(3) Furthermore, the β stabilizing element vanadium is replaced by Mo and Nb which are slower diffusing elements [37].
(4) In addition, the contents of Fe and Ni, which are very strong β stabilizers and also lead to very fast diffusion rates in α titanium [38], are reduced especially in IMI 834 to the very low levels of about 150 ppm.
(5) Owing to the reduction in volume fraction of β phase there is a potential problem: the thickness of the "β lamellae" in a colony structure is reduced in many areas to zero, i.e. only low angle boundaries are left to separate parallel α lamellae. In this case, easy slip is possible over long distances with negative consequences, especially for fatigue strength (High Cycle Fatigue, HCF, and Low Cycle Fatigue, LCF).
To create new obstacles to dislocation motion at the α/α lamellae boundaries, silicon is added to high temperature alloys (about 0.1–0.5 %). Silicon combines with titanium to form the intermetallic compound Ti_5Si_3, or in the presence of zirconium the compound $(Ti,Zr)_5Si_3$. The silicides are incoherent with respect to β and α and precipitate at the α/β lamellae boundaries and at grain boundaries, providing effective barriers to slip transfer.

(6) Since coherent precipitates are effective barriers for dislocation glide and climb, the volume fraction of Ti_3Al (α_2) particles is increased in high temperature titanium alloys, mainly owing to the addition of Sn, which adds to Al in promoting the formation of α_2, which is then $Ti_3(Al,Sn)$. As an indication of their effectiveness, the solvus temperature for α_2 in Ti–6Al–4V is around 550–600 °C, in Ti-6242 around 650 °C and in IMI 834 around 750 °C.
(7) In contrast to Ti–6Al–4V, the standard final heat treatment in Ti-6242 and IMI 834 is always an ageing treatment in the ($\alpha + \alpha_2$) phase region, i.e. 8 h 595 °C for Ti-6242 and 2 h 700 °C for IMI 834.

Processing The processing routes used to generate different microstructures, for example fully lamellar or bi-modal microstructures, in high temperature near-α titanium alloys (Ti-6242, IMI 834) are the same processing routes as those outlined in the next subsection for $\alpha + \beta$ titanium alloys. The only additional feature important for the processing route of high temperature near-α titanium alloys is the solvus temperature of the silicides in relation to the other temperatures in the processing route.

Applications The main applications of high temperature titanium alloys such as Ti-6242 and IMI 834 are blades and discs in the compressor sections of aero-engines, where the temperature exceeds 350 °C and Ti–6Al–4V cannot be used because of creep considerations. A good example is the CF6 HP compressor spool shown in Fig. 6.2, with five Ti–6Al–4V front stages followed by two Ti-6242 rear stages. Since the maximum temperature capability is about 500 °C for Ti-6242, the last stages in the HP compressors are made out of nickel-base superalloys.

Fig. 6.2 Compressor spool for GE CF6 class engine using inertia welding to connect the individual stages: front (smaller) five stages: Ti–6Al–4V; rear two stages: Ti-6242 [1]

A bi-modal microstructure is used for the Ti-6242 stages (as well as for the Ti–6Al–4V stages) because it gives the best LCF strength as well as adequate creep strength. The IMI 834 alloy can be used up to about 550 °C and is used for making blades and integrally bladed discs (blisks) in the EJ 200 aeroengine [39] and the Rolls-Royce TRENT 800 engine.

Another Ti-6242 application is the impeller shown in Fig. 6.3. Impellers are used as the last compressor stage in small (lower flow) aeroengines and in auxiliary power units (APUs).

Effect of Ni and Fe There can be considerable lot-to-lot variation in the creep strength of Ti-6242 as well as IMI-834. This variation is mainly due to variation in the concentration of Ni, which is a minor impurity that comes from vacuum distillation of Ti sponge (see Chap. 4 in this Volume) on stainless steel trays. Similar variations also appear to apply to other impurities such as Fe and Co, all at the trace impurity level. The effect of Fe has been recognized for some time, and the Fe concentration is deliberately and effectively managed by the material producers by selecting low-Fe sponge for alloy formulation.

In fact, Ni and Fe impurities are particularly troublesome in titanium production because of the use of stainless steel vessels in the Kroll reactors for making sponge, and for vacuum distillation of the sponge to remove residual $MgCl_2$ after reduction. Further, salt removal from the sponge is also done by vacuum distillation. Thus all sponge is exposed to Ni-bearing alloys during production, making trace concentrations of Ni unavoidable unless special precautions are taken.

Returning to the variation in creep behaviour, it has been shown that increasing the Ni impurity level from 0.005 to 0.035 % in Ti-6242 causes a large reduction in creep strength. This appears to be well understood in terms of Ni impurities affecting the rate-controlling creep mechanism, which is diffusion-controlled dislocation motion in the α phase [41–47]. Consistent improvement in the creep strength of high temperature alloys requires the use of materials with the lowest commercially feasible Ni and Fe levels.

Fig. 6.3 Impeller used in a small engine for regional jets, diameter 35 cm. The alloy is Ti-6242 with a bi-modal microstructure [1]

A special consideration for low temperature (up to about 150–200 °C) applications of near-α alloys in aeroengines is ***dwell fatigue cracking***. This can occur when hold times at high load levels are part of the service fatigue history. Dwell cracking is a well-known and major concern for front-engine discs made from alloys such as Ti-6242, IMI 685, and IMI 834. It was first encountered in 1972 with two *in-service* fan disc failures [47]. Although not fully understood, the cracking involves creep (low temperature) as well as fatigue, and microtexture appears to play a major role. More details can be found in the specialist literature.

6.2.3 α + β Titanium Alloys

6.2.3.1 Processing and Microstructures of α + β Titanium Alloys

α + β alloys have at least two phases (α and β) and have good combinations of strength and high temperature properties. This is why these alloys have been so popular. Correct microstructures are essential, which is all the more important because titanium alloy microstructures are very sensitive to processing.

Three distinctly different types of microstructures can be obtained in α + β alloys by changing the thermomechanical processing route: so-called bi-modal (duplex) microstructures containing equiaxed primary α (α_p) in a lamellar α + β matrix; fully equiaxed structures; and fully lamellar structures. A common but less narrowly defined microstructure is the so-called mill-annealed condition.

Central to the processing of titanium alloys is the deformation and resulting morphology of the alpha/beta phase. An equiaxed α morphology is obtained by α + β processing and α + β solution treatment, whereas a fully lamellar α (transformed β) microstructure is obtained from heating and/ or processing in the β phase field.

Bi-modal microstructures The processing route for obtaining the bi-modal (duplex) microstructures is shown schematically in Fig. 6.4, where the process is divided into four different steps: homogenization in the β phase field (I), deformation in the (α + β) phase field (II), α-phase recrystallization in the (α + β) phase

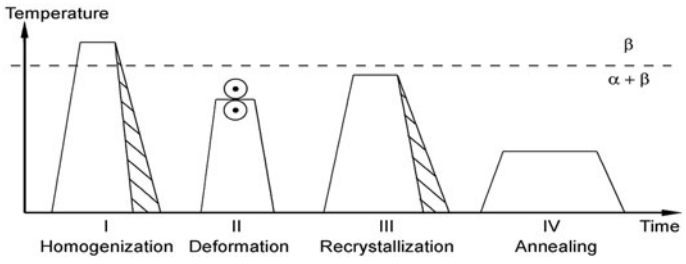

Fig. 6.4 Schematic processing route for bi-modal microstructures of α + β titanium alloys

field (III) and final ageing and/or stress relieving treatment (IV). Table 6.3 summarizes the important parameters of this processing route and the resulting microstructural features.

A critical parameter in the processing route is the cooling rate from the homogenization temperature in the β phase field (step I) because this cooling rate determines the width of the α lamellae. These are then deformed in step II and recrystallized in step III.

The relation between the prior α lamellae width resulting from step I and the equiaxed primary α + β size is illustrated in Fig. 6.5, where two bi-modal structures are compared. The faster the cooling rate, the finer are the α lamellae, the primary $\alpha(\alpha_p)$ grain size and the transformed β grain size.

Table 6.3 Important processing step parameters and resulting microstructural features for bi-modal microstructures

Step	Important parameters	Microstructural features
I	Cooling rate	Width of α lamellae (→ α_p size)
II	Deformation temperature Deformation degree Deformation mode	– Texture type – Texture intensity – Dislocation density – Texture symmetry
III	Annealing temperature Cooling rate	– Vol.% of α_p (→ β grain size) –Alloy element partitioning Width of α lamellae
IV	Annealing temperature	– Ti_3Al in α – Secondary α in β

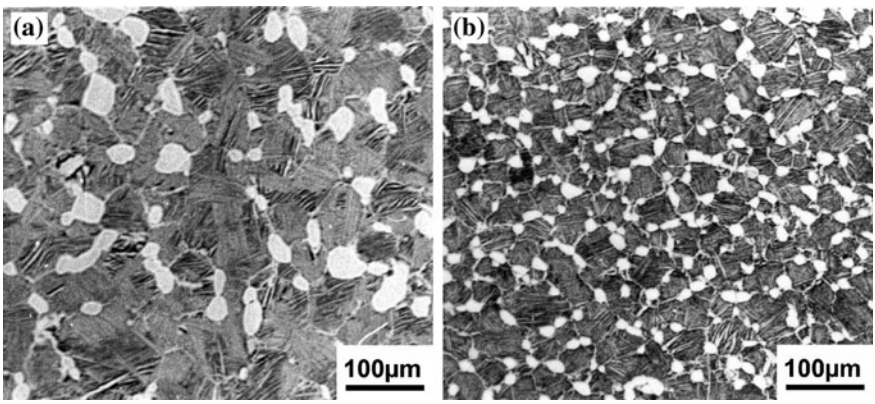

Fig. 6.5 Bi-modal microstructures (optical) of the IMI 834 alloy cooled differently from the β phase field in step I of the processing route: **a** bi-modal 1, slow cooling rate, **b** bi-modal 2, fast cooling rate

In bi-modal microstructures the cooling rate from the recrystallization annealing temperature in the (α + β) phase field (step III in Fig. 6.4) mainly influences the width of the individual α lamellae (Table 6.3), whereas the α colony size and the length of the continuous α layers at β grain boundaries are largely determined by the β grain size. Within the normal range of commercial cooling rates of about 30−600 °C/min, the α colony size in bi-modal microstructures is about equal to the β grain size. Slower cooling rates increase both the size and volume fraction of α_p.

Fully equiaxed microstructures There are two possibilities to obtain a fully equiaxed microstructure. In the first case, the processing route is identical to the processing route for obtaining a bi-modal microstructure up to the recrystallization process in step III:

(1) If the cooling rate from the recrystallization annealing temperature is sufficiently low, only the α_p grains will grow during the cooling process and no α lamellae are formed within the β grains, resulting in a fully equiaxed structure with the equilibrium volume fraction of β phase located at the "triple-points" of the α grains. In this case the α grain size will be fairly large and always larger than the α_p size of a bi-modal structure (which would have resulted from faster cooling).
An example for such a fully equiaxed microstructure is shown in Fig. 6.6.

(2) The second possibility to obtain a fully equiaxed microstructure is to recrystallize in step III of the processing route (Fig. 6.4) at such a low temperature that the equilibrium volume fraction of α phase at that temperature is high enough to form the fully equiaxed microstructure directly from the deformed lamellar structure.

Using this second processing route with the (low) recrystallization annealing temperature (for example, for Ti–6Al–4V between 800−850 °C), smaller α grain

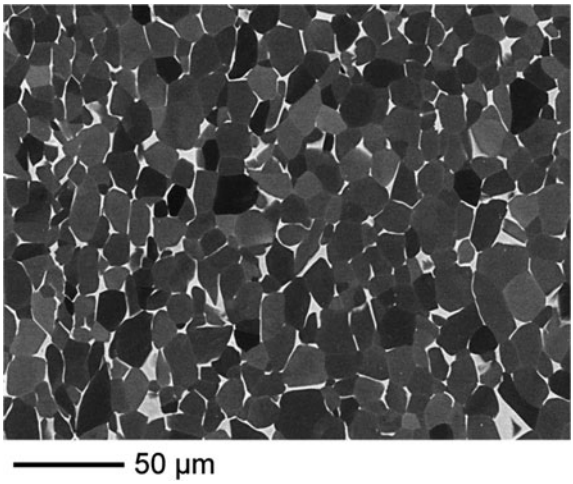

Fig. 6.6 Fully equiaxed microstructure obtained in Ti–6Al–4V

sizes can be achieved provided a higher degree of deformation is used as compared to method (1). For example, for Ti–6Al–4V a recrystallization annealing temperature of 800 °C enables fully equiaxed microstructures with α grain sizes of about 2 μm or less [26] to be obtained.

N.B: Fully equiaxed microstructures can be changed to bi-modal microstructures by simply reheating the material to a temperature in the (α + β) phase field that corresponds to the desired α_p volume fraction and subsequently cooling with a sufficiently high rate to form α lamellae within the β grains.

The mill-annealed condition mentioned earlier is obtained by omitting the recrystallization step III (see Fig. 6.4). Consequently, the details of the deformation procedure in step II (number of times it is reheated during deformation, soaking time, the amount of deformation and the cooling rate after deformation, etc.) determine the details of the resulting microstructure, especially the degree of recrystallization. Since the details of the deformation procedure are beyond the control of the customer or end-user, and these details will vary between producers or even between different lots, the mill-annealed condition is not a well-defined microstructural condition.

Fully lamellar microstructures Lamellar microstructures can be obtained fairly easily in the final steps of the processing route by an annealing treatment in the β phase field (β recrystallization). Hence this microstructure is often also called "β annealed". The processing steps are similar to those in Fig. 6.4, but the temperatures are different. The deformation process (step II) can be done by forging or rolling, either in the β phase field or in the (α + β) phase field, as shown in Fig. 6.7, and the annealing step (shown as recrystallisation step III in Fig. 6.7) is carried out in the β phase field.

In industrial practice the material is usually first deformed in the β phase field to refine the coarse ingot microstructure, to homogenize the material, and because of the lower flow stress. The material is then deformed in the (α + β) phase field to avoid large β grain sizes. Similarly, the recrystallization temperature in step III is usually kept within 30−50 °C above the β transus to maintain control of the β grain

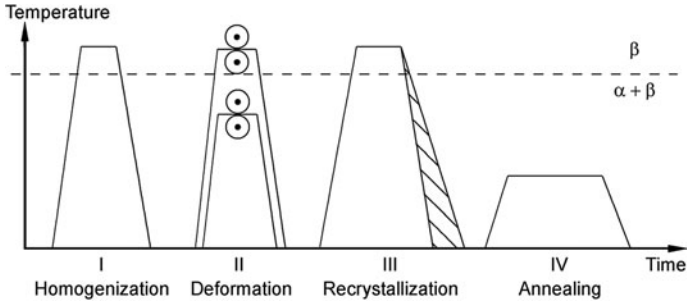

Fig. 6.7 Processing route to obtain fully lamellar microstructures in α + β alloys

size. As a result, the β grain size of fully lamellar microstructures is typically about 600 μm.

Another type of fully lamellar microstructure, namely a so-called β processed condition, is mentioned here, although for α + β alloys this condition is not used extensively in commercial applications. β processing (which is a very common processing route for β alloys) involves omitting β recrystallization, and the material remains therefore in an unrecrystallized condition.

6.2.3.2 Mechanical Properties of α + β Titanium Alloys

The mechanical properties emphasized in this section are tensile, fatigue and fracture toughness. A qualitative summary of the basic microstructure/property correlations is shown in Table 6.4.

The qualitative trends (+, 0, −) in Table 6.4 indicate the directions in which a specific mechanical property will change when a microstructural feature is changed according to the table footnotes. For the tensile properties the 0.2 % yield stress and fracture strain are used for the correlations. The HCF strength at 10^7 cycles is taken as a measure of the resistance to fatigue crack nucleation.

Bi-modal microstructures For the whole range of commercial cooling rates (30–600 °C/min) the α colony size of bi-modal microstructures is about equal to the β grain size, and therefore much smaller than in fully lamellar microstructures.

Based on the effect of slip length on mechanical properties of fully lamellar structures, it can be postulated that if the slip length would be the only major parameter governing the mechanical properties of bi-modal microstructures, they should have a higher yield stress, a higher ductility and a higher HCF strength than fully lamellar microstructures, when compared for the same cooling rate.

In fact, Table 6.4 indicates that this is not so. The reason is that there is another important factor which complicates the situation. That is the alloy element partitioning effect, which increases with increasing volume fraction of α_p. The HCF strength (crack nucleation resistance) is usually reduced with increasing α_p volume

Table 6.4 Qualitative correlations between important microstructural parameters and mechanical properties for α + β titanium alloys [1]

Microstructural features	0.2 % YS	ε_F	HCF	K_{1c}	Creep strength (0.2 %)
Small α colonies, α lamellae[a]	+	+	+	−	±
Bi-modal structure[b]	+	+	−	−	−
Small α grain size[c]	−	+	+	−	−
Ageing (α_2); oxygen	+	−	+	−	+
Secondary α in β	+	−	+	0	+

[a]Compared to coarse lamellar structure
[b]Compared to fully lamellar structure with same cooling rate
[c]Compared to large α grain size of fully equiaxed microstructures

fraction. The fatigue cracks are nucleated in the lamellar grains of the bi-modal structure because the crack path is more irregular in this latter condition and these lamellar grains are softer than α_p as a consequence of the alloy element partitioning effect.

The fracture toughness of bi-modal microstructures of the Ti–6Al–4V alloy is only slightly higher than the fracture toughness of the fine lamellar microstructure, but much lower than the toughness of the coarse lamellar structure. A detailed discussion is beyond the scope of this chapter: the reader is referred to the Bibliography. Also, it is important to note that the creep properties of a lamellar structure are better than those of bi-modal structures: again see the Bibliography for a detailed discussion.

Fully equiaxed microstructures The mechanical properties of fully equiaxed microstructures of α + β titanium alloys are primarily influenced by the α grain size. It should also be emphasized that fully equiaxed microstructures of α + β titanium alloys are similar to the microstructures of CP titanium and other α titanium alloys. Therefore the general correlation between microstructure and mechanical properties is also similar.

The effect of α grain size on HCF strength of fully equiaxed microstructures is demonstrated in Fig. 6.8 for the Ti–6Al–4V alloy. It can be seen that high HCF strength values can be achieved with small α grain sizes. The corresponding yield stress values are 1120 MPa (2 μm grain size), 1065 MPa (6 μm grain size) and 1030 MPa (12 μm grain size), respectively. The tensile ductilities of these fully equiaxed microstructures are generally very high, i.e. equal to or higher than those of bi-modal microstructures on a strength-corrected basis.

The LCF strength is lower for fully equiaxed microstructures as compared to bi-modal microstructures. A similar evaluation of the effect of α grain size on LCF strength of fully equiaxed microstructures suggests that the LCF strength will

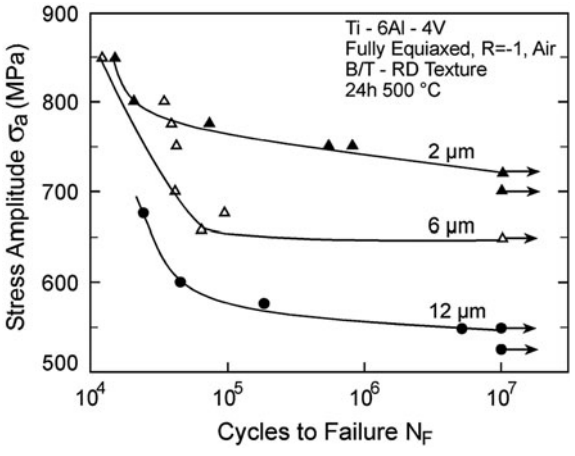

Fig. 6.8 Effect of α grain size on HCF strength of Ti–6Al–4V with fully equiaxed microstructures

increase with decreasing α grain size because of increased ductility: this follows from the Coffin-Manson Law prediction about LCF strength and ductility.

The effect of α grain size on fracture toughness of fully equiaxed microstructures has been investigated by comparing microstructures with 2 and 12 μm grain sizes. The fracture toughness values were 45 and 65 MPa $\sqrt{m}$, respectively. This result demonstrates the same tendency as found for lamellar microstructures (discussed next with respect to Fig. 6.8), namely, that the crack front roughness has a major influence on the fracture toughness.

Fully lamellar microstructures The most influential microstructural parameter for the mechanical properties of lamellar microstructures is the α colony size, which is the effective slip length and is controlled by the cooling rate from the β heat treatment temperature. With increasing cooling rate the α colony size decreases with a commensurate reduction in effective slip length and a corresponding increase in yield stress.

In the commercially feasible cooling rate regime (up to 1000 °C/min), the effect on yield stress is only moderate (50−100 MPa), whereas a large increase in yield stress is observed when the colony structure is changed to a martensitic type of microstructure (slip length and "colony" size equal to the width of individual α plates).

With increasing cooling rate the tensile ductility increases at first, consistent with the effect of decreased slip length. However, the ductility reaches a maximum and then declines. The ductility maximum corresponds to a change in fracture mode. For low cooling rates a ductile *transcrystalline* microvoid dimple type of fracture is observed, whereas at high cooling rates a ductile i*ntercrystalline* dimple type of fracture occurs along the continuous α layers at prior β grain boundaries. The effect of the continuous α layers on ductility is related to preferential plastic deformation in this lower strength region and concomitant early microvoid nucleation.

The magnitude of the ductility decline depends primarily on the strength difference between the continuous α layers and the matrix, and also the grain boundary length: a larger β grain size is detrimental.

The HCF strength depends primarily on the resistance to dislocation motion. Consequently, the HCF strength dependence on α colony size is qualitatively similar to that of the yield stress. It should be noted that for fully lamellar microstructures the absolute values for both the HCF strength and the yield stress depend, in addition to the cooling rate effect, on the details of the final annealing/ageing treatment (step IV in Fig. 6.7).

The fracture toughness of α + β titanium alloys usually increases with increasing α colony size owing to a rougher crack front profile. Figure 6.9 shows an example of the difference in crack path for a coarse lamellar microstructure (1 °C/min cooling rate) and a fine lamellar microstructure (8000 °C/min cooling rate) in Ti–6Al–4V. The corresponding fracture toughness values were 75 MPa $\sqrt{m}$ for the coarse structure and 50 MPa $\sqrt{m}$ for the fine structure. In other words, increasing crack front roughness increases the fracture toughness.

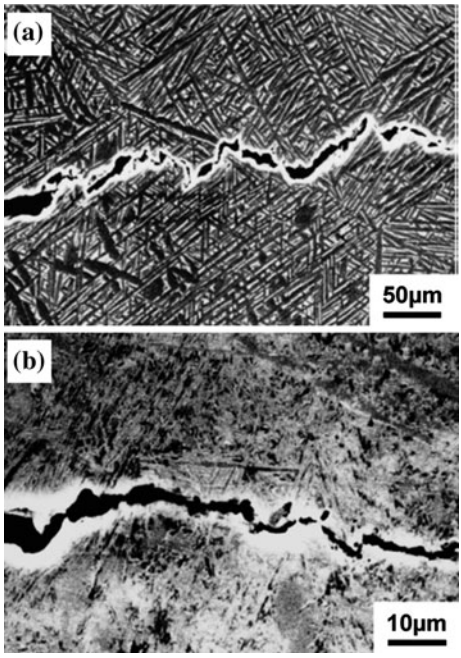

Fig. 6.9 SEM micrographs of crack paths in the centres of fracture toughness specimens of Ti–6Al–4V: **a** coarse lamellar (higher toughness), **b** fine lamellar (lower toughness). *Note the difference in magnifications*: the crack path in (**a**) is much rougher

Titanium alloy Ti6Al4V ELI grade Ti6Al4V ELI grade is similar to Ti6Al4V except that the ELI grade has reduced levels of oxygen, nitrogen, carbon and iron. ELI stands for "Extra Low Interstitials", referring to oxygen, nitrogen and carbon.

The essential difference between Ti6Al4V ELI (grade 23) and Ti6Al4V (grade 5) is the reduction of oxygen content to 0.13 % (maximum) in grade 23. This confers improved ductility and fracture toughness, with some reduction in strength.

The improved properties, high specific strength (strength/density), good stress corrosion resistance and machinability are why Ti6Al4V ELI is extensively used for aerospace cryogenic applications (e.g. spacecraft pressure vessels and fuel tanks).

Ti6Al4V ELI has also been widely used in fracture critical airframe structures and for offshore tubulars. The mechanical properties for fracture critical applications can be enhanced, if necessary, by special processing and heat treatment.

6.2.3.3 Applications of α + β Titanium Alloys

This class of titanium alloys is the most used. Within this class the worldwide production of Ti–6Al–4V is the largest.

Airframe structures A major application area of α + β titanium alloys is in heavily loaded aircraft structural parts. For such applications, α + β titanium alloys can be

selected over other competing metallic materials, such as high strength aluminium alloys, because of higher yield strength and elastic modulus (and also higher specific strength and stiffness), fatigue strength, better corrosion resistance and higher temperature capability. Figures 6.10 and 6.11 show two heavy Ti–6Al–4V forgings for aircraft.

The most economically effective processing route for large forgings typically consists of forging in the ($\alpha + \beta$) phase field followed by mill-annealing. The mill-annealed microstructure gives generally faster fatigue crack propagation rates than a fully lamellar microstructure, which can be obtained by β annealing, however at increased cost. Although β annealing requires fixtures to support the part, the benefits of improved crack propagation resistance are in some cases sufficient to justify the added cost. This is sometimes done for fracture critical aircraft structural components such as bulkheads, cockpit window frames and attachment fittings for

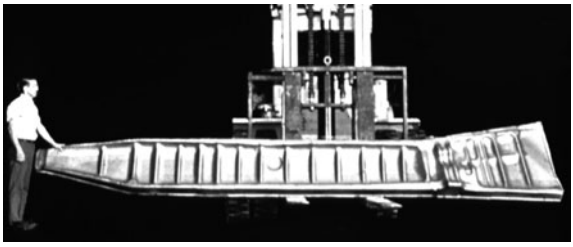

Fig. 6.10 Large Ti–6Al–4V forging for Boeing 747 landing gear [1]

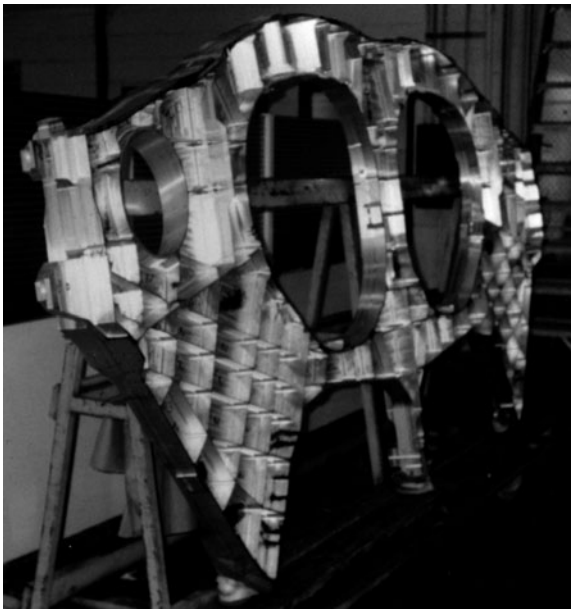

Fig. 6.11 Machined bulkhead forging for a twin engine military aircraft, [1]

the fin and horizontal stabilizers. β-annealed plate is used extensively for the Lockheed Martin F-35 Joint Strike Fighter (JSF).

Castings of Ti–6Al–4V already possess fully lamellar microstructures, but also have size limitations resulting from the casting furnace equipment and the hot isostatic press (HIP) facilities required for airworthiness certification of premium quality castings. Nevertheless, fairly large castings have been proposed for use in static property limited aircraft structural components. In such applications the large section sizes mean that the solidification rate will be quite slow. This results in a fairly coarse lamellar microstructure with excellent macrocrack fatigue crack growth resistance and high fracture toughness.

Aeroengines Another major application area of α + β titanium alloys is for rotating and non-rotating parts in aeroengines. The major limitation of Ti–6Al–4V is the maximum usage temperature of about 300 °C, which restricts this alloy to the fan stage (Fig. 6.12), the low pressure (LP) compressor section and the front stages in the high pressure compressor (HPC). Further back in the HPC the higher temperatures require creep-resistant high temperature titanium alloys (Ti-6242, Titan 29A and IMI 834), e.g. Figs. 6.13 and 6.14.

Fig. 6.12 Large fan blades (length of the larger blade about 1 m) of Ti–6Al–4V forged in the (α + β) phase field and recrystallized to a bi-modal microstructure [1]

Fig. 6.13 Aeroengine high pressure compressor rings made of Titan 29A

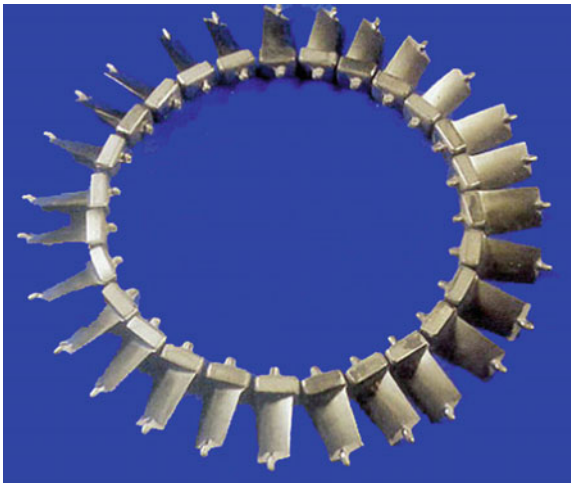

Fig. 6.14 Aeroengine high pressure compressor blades made of Titan 29A

Ti–6Al–4V is also used for the new technology of manufacturing integrally bladed rotors (IBR), either by direct attachment of the blades to the disc using solid-state linear friction welding, or by machining the rotor from a single-piece forging.

6.2.4 β Titanium Alloys

6.2.4.1 Introduction: General Characteristics

In contrast to α + β alloys, β alloys do not transform martensitically upon quenching to room temperature: instead they consist of metastable β. The α phase can be precipitated from the metastable β phase as very fine, undeformable particles (platelets) with a high volume fraction. Thus the main characteristic of β alloys is that they can be hardened to much higher yield stress levels than α + β alloys. Another advantage is that they can be processed at lower temperatures than α + β alloys, and some heavily stabilized β alloys are even cold deformable. Further, the corrosion resistance of β alloys is equal to or better than that of α + β alloys, and they are especially good in environments where hydrogen pickup is possible, because β has a higher hydrogen tolerance than α. In view of these advantages the usage of β alloys has been slowly but steadily increasing in recent years.

A distinction can be made between so-called "high strength" and "heavily stabilized" β alloys:

(1) High strength alloys have chemical compositions close to the β/α + β phase boundary. In the aged condition they therefore contain a high volume fraction of α phase.

(2) Heavily stabilized alloys are located more to the right in the pseudo-binary phase diagram. These alloys contain a much lower volume fraction of α phase and the maximum achievable strength is therefore lower.

Typical examples for the first group of alloys are Ti-6246, Ti-17, β-CEZ and Ti-10-2-3. Examples of the second group are Beta 21S, Ti-15-3 and Beta C. The main emphasis in this subsection is on the group of high-strength β alloys, and most examples are from this group, which are therefore simply referred to as "β alloys". Where heavily stabilized β alloys are discussed, this will be explicitly stated.

6.2.4.2 Processing and Microstructures

Beta-annealed microstructures The basic processing route for β-annealed microstructures is shown in Fig. 6.15. It can be seen that the β-annealed microstructure is obtained in a simple way, i.e. recrystallization in the β phase field (step III) and ageing in the (α + β) phase field (step IV) to precipitate α as fine α platelets. Such a microstructure is shown in Fig. 6.16.

The main characteristic of all β alloys is that the α phase nucleates preferentially at β grain boundaries and forms a continuous α layer. Adjacent to this continuous α layer is a so-called PFZ (precipitate-free zone) which does not contain any α platelets, and which is therefore soft with respect to the age-hardened matrix.

The strength difference between the PFZs and the matrix (i.e. yield stress) and the slip length in the PFZs (i.e. β grain size) are important for the mechanical properties. Both of these parameters are influenced by alloy composition, such that the effect of the continuous α layers is large for high strength β alloys and smaller for heavily stabilized β alloys. This is the reason why high strength β alloys are not used in the β-annealed condition. On the other hand, heavily stabilized β alloys are commonly used in the β-annealed condition.

Table 6.5 summarizes the important processing parameters and resulting microstructural features of heavily stabilized β alloys. An important parameter of

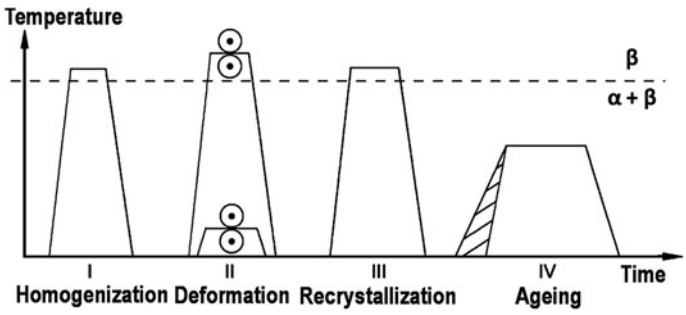

Fig. 6.15 Processing route for β-annealed microstructures of heavily stabilized β titanium alloys [1]

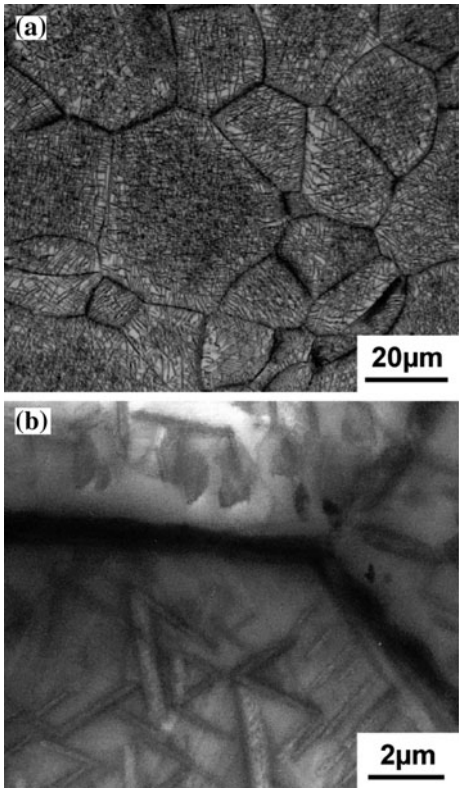

Fig. 6.16 β-annealed plus aged microstructure of a heavily stabilized β alloy, Beta 21S [1]: **a** optical and **b** TEM metallographs showing α precipitation within the grains and at the grain boundaries and narrow precipitate-free zones (PFZ) near the grain boundaries

Table 6.5 Important processing parameters and resulting microstructural features for β-annealed microstructures of heavily stabilized β alloys [1]

Processing step (see Fig. 6.15)	Important parameters	Microstructural features
III	Recrystallization temperature	β grain size
IV	Heating rate	Distribution of α platelets
	Ageing temperature	Size and vol.% of α platelets GB α layer

the ageing treatment (step IV in Fig. 6.15) is the choice of the ageing temperature, because this determines the volume fraction of α platelets which influences the yield stress level. (Since the growth of the α platelets is diffusion controlled, the ageing *temperature* is much more important in step IV than the ageing *time*.) However, formation of the continuous α layers at β grain boundaries during the ageing treatment cannot be avoided.

It is sometimes difficult for heavily stabilized β alloys (especially for relatively high ageing temperatures) to obtain a homogeneous distribution of α platelets by

the normal one-stage ageing treatment shown in Fig. 6.15. This is because (i) the necessary formation of the ageing precursors (ω or β′) can be too sluggish to occur during heating to the ageing temperature, and (ii) the ageing temperature is above the stability range for ω or β′. In this case a pre-ageing at lower temperatures can create a more homogeneous distribution of α platelets [48]. This means that there is a two-stage ageing step (step IV in Fig. 6.15).

After homogenization (step I), the deformation (step II) can be done either in the β phase field or in the (α + β) phase field, see Fig. 6.15. The latter has the advantage of creating smaller β grain sizes in the recrystallization step III. The grain size of β-annealed microstructures is somewhat smaller than the β grain size in fully lamellar microstructures of α + β alloys. A typical grain size of β alloys is about 400 μm as compared to about 600 μm for α + β alloys for equivalent processing histories and for a recrystallization temperature of 30–50 °C above the β transus. The smaller grain size of β alloys is a result of the lower β transus. The most important parameter in step III is the cooling rate from the recrystallization temperature because it controls the width and extent of the continuous α layers at β grain boundaries. **N.B**: even for fast cooling rates in commercial practice (e.g. 600 °C/min), formation of the continuous α layers cannot be avoided. Since the total volume fraction of α (coarse α plates plus fine α platelets and grain boundary α) is fixed by the alloy chemistry, the volume fraction of coarse α plates has a direct influence on the volume fraction and size of the fine α platelets and therefore on the resulting yield stress level of the material.

β processed microstructures To obtain β processed microstructures the recrystallization step III in Fig. 6.15 is omitted, with the intention of creating an unrecrystallized structure with highly deformed β grain boundaries. The α layers which form on the β grain boundaries during cooling from the β deformation temperature will then take on the local shape of the deformed grain boundaries. An example is given in Fig. 6.17a for the Ti-6246 alloy. This shows that the α layers are still fairly continuous but have a pronounced wavy shape. In other cases the α layers are broken up more into individual segments on most β grain boundaries with only a few long segments remaining on some boundaries. Irrespective of processing history, it is nearly impossible to completely avoid the α layers. This is because the β grain boundaries are strong heterogeneous nucleation sites for α formation.

Since the final deformation process must be a continuous operation without reheating, good control of the processing temperature and time is necessary. Critical parameters are the total time of the process, determined by deformation rate, amount of deformation and any holding times between deformation steps and after the deformation process.

The deformation mode determines the shape of the unrecrystallized β grains, for example ellipsoidal from unidirectional rolling, pancake-shaped from cross-rolling, or axisymmetric from upset forging. Consequently, the mechanical properties which are influenced by the α layers will be anisotropic.

Ageing results in small α platelets within the β grains and between the coarse α plates formed during cooling after the deformation step, see Fig. 6.17b.

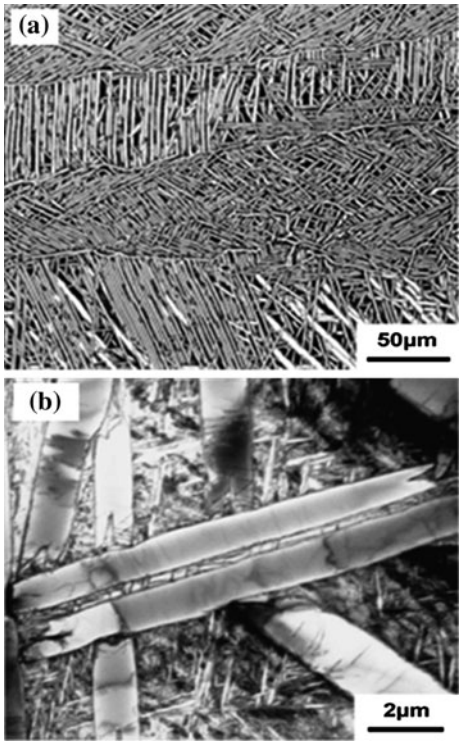

Fig. 6.17 β processed microstructure of Ti-6246 alloy [1]: **a** optical image of deformed β grain boundaries outlined with α; **b** TEM micrograph showing coarse primary α and fine secondary α within a grain

Through-transus processed microstructures Extensive development work on the through-β-transus processing route has been done for the β-CEZ alloy [49]. The intention of this processing route is to change the continuous α layers at β grain boundaries to individual globular α particles. In the through-transus processing route the deformation step II starts above the β transus and finishes below the beta transus. This process is otherwise identical to that for β processed materials, i.e. an unrecrystallized β grain structure is anticipated by omitting the recrystallization step III.

The control of deformation temperature and time in step II is even more critical for the through-transus processing route than for the β processing route [50]. The deformation time in the (α + β) phase region in step II should be long enough to cross the TTT boundary line for α precipitation at the deformed β grain boundaries, but the deformation process should be finished before crossing the TTT boundary line for α precipitation in the β matrix [50].

Another issue associated with through-transus processing is that the deformation time must be long enough to allow α precipitation to occur at β grain boundaries, but the time in the β phase field must be restricted to avoid recrystallization of the deformed β grains [50]. The only advantage in the through-transus processing route as compared to β processing is that the cooling rate after the deformation process is

less critical because the α phase is already precipitated at the β grain boundaries in the necklace microstructure (see next paragraph).

Examples of through-transus microstructures, obtained from Ti-6246 alloy, are given in Fig. 6.18. The as-deformed microstructure is shown in Fig. 6.18a. This kind of microstructure has been called a "necklace" microstructure by CEZUS for their β-CEZ alloy [51]. The higher magnification micrograph in Fig. 6.18b for the fully heat treated alloy shows globular α particles at the β grain boundaries and α plates within the grains.

Bi-modal microstructures The benefit of a bi-modal microstructure is to avoid the continuous α layers at the boundaries of large β grains by creating a small enough β grain size that any α layers that form have only a negligible effect on mechanical properties. The processing route for obtaining a bi-modal microstructure is shown schematically in Fig. 6.19. The important processing parameters and the resulting microstructural features are summarized in Table 6.6.

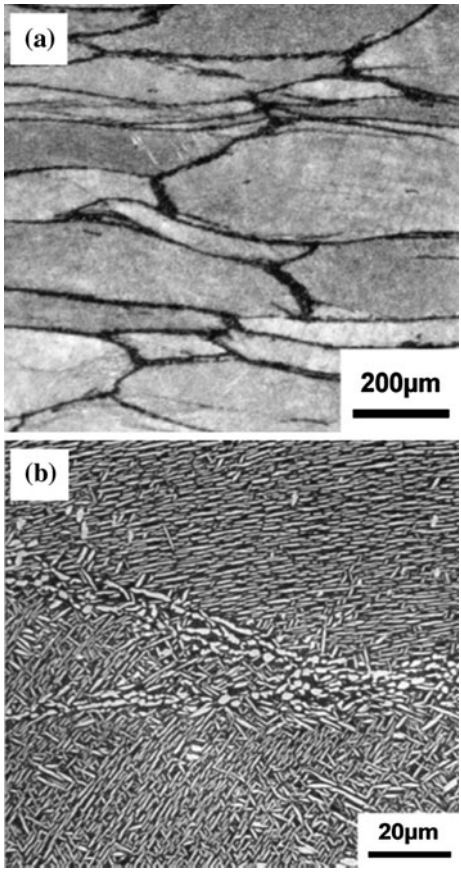

Fig. 6.18 Optical microstructure of a through-transus processed microstructure ("necklace" microstructure) of Ti-6246 alloy [1]: **a** as-deformed; **b** aged

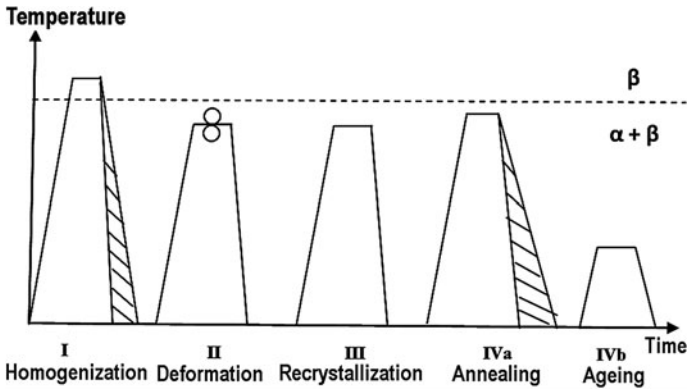

Fig. 6.19 Processing route for bi-modal microstructures of β alloys

Table 6.6 Important processing parameters and resulting microstructural features for bi-modal microstructures of β alloys

Processing step (see Fig. 6.19)	Important parameters	Microstructural features
I	Cooling rate	GB α layer
II	Deformation degree	Dislocation density
III	Annealing temperature	Vol.% of α_p (→ β grain size and vol.% of α plates in step IVa)
IVa	Annealing temperature and cooling rate	Size and vol.% of α plates (→ vol.% of α platelets in step IVb)
IVb	Ageing temperature	Size and vol.% of α platelets

When selecting the intermediate annealing temperature for bi-modal microstructures it should be realized that the volume fraction of coarse α plates is determined by the temperature difference between the recrystallization annealing temperature (formation of equiaxed primary α) and the intermediate annealing temperature.

6.2.4.3 Mechanical Properties of β Titanium Alloys

Microstructure and mechanical properties A qualitative summary of the microstructure/property correlations is shown in Table 6.7. The symbols (+, 0, −) indicate the direction in which the mechanical properties change when the microstructure is changed. This table compresses much comparative information as follows:

Table 6.7 Qualitative correlations between important microstructural parameters and mechanical properties for β titanium alloys (both high strength and heavily stabilized) [1]

Microstructural features	0.2 % YS	ε_F	HCF	K_{1c}
GB α layers in β-annealed structure	0	−	−	+
Bi-modal structure[a]	0	+	+	−
"Necklace"[a] or β processed structure[b] (longitudinal direction)	0	+	+	+
	0	−	−	+
Decreasing age-hardening	−	+	−	+
Small β grain size in β-annealed structure[c]	0	+	+	−

[a]Compared to β-annealed structure
[b]Compared to bi-modal structure
[c]Only applies to heavily stabilized alloys

(1) The first row gives the overall effects of continuous grain boundary (GB) α layers in ***β-annealed*** structures.
(2) The second row compares the properties of ***bi-modal*** structures with those of ***β-annealed*** structures, both with continuous α layers.
(3) The third row has two sub-rows (a and b) for comparing the effects of unrecrystallized microstructures with (a) ***β-annealed*** structures and (b) ***bi-modal*** structures.

This overall comparison of mechanical properties is discussed separately for strength, fatigue strength and fracture toughness in the following text; and on the basis of final ageing resulting in a constant yield stress level.

Tensile properties The mechanical properties of high-strength β alloys are dominated by the preferential plastic deformation along the continuous α layers at β grain boundaries. The unacceptably low ductility of high strength β alloys in the β-annealed condition can be drastically improved by α + β processing to a bi-modal microstructure with a small β grain size [52], see column "ε_F" in Table 6.7.

The β processed (unrecrystallized) condition shows high tensile anisotropy, with the lowest yield stress in the 45° test direction as compared to the other two directions: this is illustrated in Table 6.8. This yield stress anisotropy can be

Table 6.8 Tensile properties of β-CEZ alloy [1]

Processing and orientation		0.2 % YS (MPa)	UTS (MPa)	σ_F (MPa)	T.E. (%)	RA (%)
β annealed	L	1180	1280	1415	4	10
Bi-modal	L	1200	1275	1660	13	34
β-processed	L	1190	1275	1480	10	16
	45°	1145	1200	1220	2	2
	T	1185	1280	1410	6	10

explained from the crystallographic texture of the β matrix. Also the fracture properties are dominated by the angle of the tensile stress axis with the elongated β grain boundaries containing α layers.

Fatigue Properties Figures 6.20 and 6.21 give examples of the HCF properties of β-CEZ:

(1) Figure 6.20 compares the fatigue properties of β processed β-CEZ for three test directions. The HCF strength for the ST test direction was higher than for the L direction, which is a remarkable result. On the other hand, the 45° test direction resulted in the lowest fatigue strength, and this correlates with the lowest yield stress (see Table 6.8).

(2) Figure 6.21 compares the fatigue properties of β-CEZ for three different microstructures, with the added complication of a 45° test direction for the β processed material. The fine-grained bi-modal microstructure gave the highest fatigue strength; the coarse-grained β-annealed microstructure was intermediate; and the β processed material again gave the lowest fatigue strength when tested in the 45° direction.

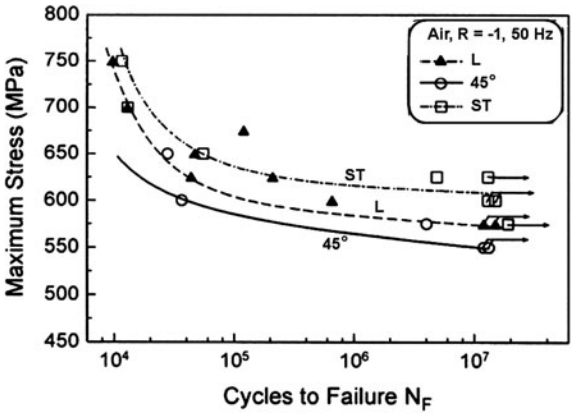

Fig. 6.20 *S–N* curves of a β processed forged rectangular slab of β-CEZ [1]

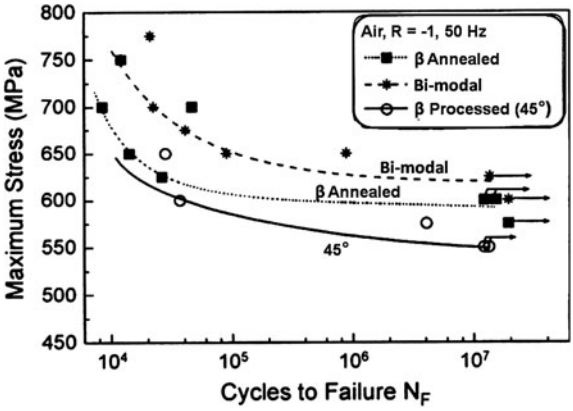

Fig. 6.21 *S–N* curves for different microstructures in β-CEZ [1]

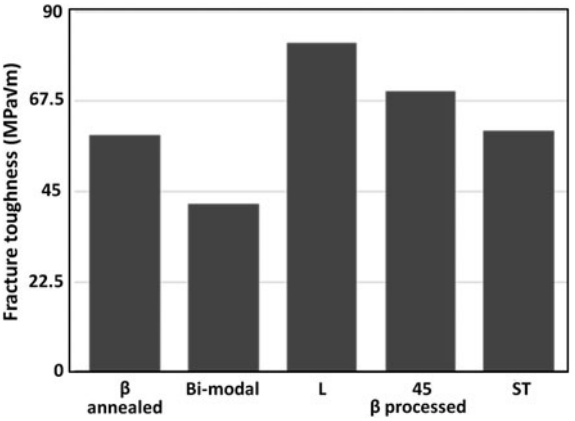

Fig. 6.22 Fracture toughness of Ti-6246 as a function of different processing and heat treatment conditions [1]

The HCF fatigue behaviour of Ti-6246 followed the same trends. A detailed explanation is beyond the scope of this chapter and is given in Refs. [1, 34].

Fracture Toughness The fracture toughness values of the β-annealed and bi-modal microstructures as well as those of the β processed condition for the three different testing directions (L, 45°, ST) are shown in Fig. 6.22 for Ti-6246.

As can be seen, the fracture toughness of the β-annealed condition is much higher than that of the bi-modal condition. This is because the crack tip plastic zone that forms during the onset of crack extension tends to follow β grain boundaries, more specifically along the α layers at β grain boundaries, and the resulting crack deflection contributes to the increased toughness. In contrast, the fine-grained bi-modal surface topography resulted in a much lower fracture toughness value [1].

In more detail, the data for β-annealed material in Fig. 6.22 and the fractographic observations [1] show that the influence of crack front profile (increased roughness lowers the *crack driving force*) is substantial and more than compensates for the easier crack path (lower *crack growth resistance*) within the weak PFZ zones along the β grain boundaries. This is why there is a (+) symbol for K_{Ic} in the first row of Table 6.7.

Returning to Fig. 6.22, the fracture toughness of the β processed material showed the highest value for the L test direction, followed by the 45° test direction and then the ST direction. This trend, notably the lowest toughness in the ST direction, is common for thick-section products of high-strength alloys.

6.2.4.4 Applications of β Titanium Alloys

Aerospace usage of β titanium alloys is increasing mainly at the expense of the widely used α + β Ti–6Al–4V alloy, and this is because higher strengths are achievable from β titanium alloys with retention of good ductility and acceptable fracture toughness.

Large and small forgings The Boeing 777 aircraft was the first commercial airplane for which the volume of β alloys exceeded the volume of Ti–6Al–4V. The main reason was use of the high strength β alloy Ti-10-2-3 in the landing gear structure, see Fig. 6.23a. Many parts in the landing gear structure are Ti-10-2-3, except for the outer and inner cylinders and the axles, all being steel. The biggest single item was the truck beam with a length of about 3 m and a diameter of about 0.34 m. The truck beam was initially fabricated by forging three pieces and joining them by electron beam welding. Later, the beam was made as a one-piece forging. The published forging practice for the Ti-10-2-3 alloy is β forging followed by α + β forging to plastic strains of about 15–25 % [35].

Smaller parts of Ti-10-2-3 alloy are easier to forge, and some examples of precision forgings are shown in Fig. 6.23b. These parts are used in the Boeing 777 cargo handling system. The cost advantage of Ti-10-2-3 over Ti–6Al–4V lies in the lower forging temperature and tooling costs [36]. Yet another application using relatively large Ti-10-2-3 forgings is the Super Lynx helicopter rotor head shown in Fig. 6.24.

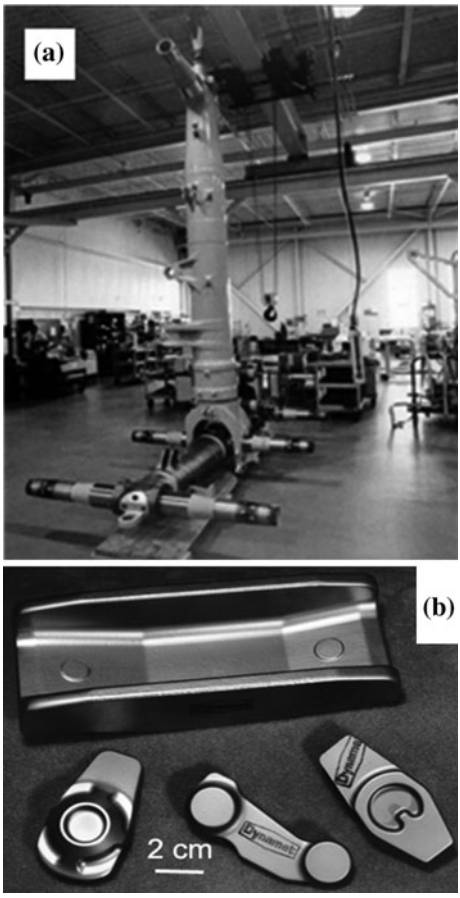

Fig. 6.23 Boeing 777 landing gear and some small parts required in large numbers for an aircraft: all made using Ti-10-2-3 [1]

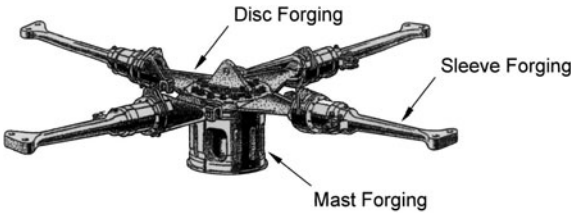

Fig. 6.24 Helicopter rotor using Ti-10-2-3 forgings [1]

Springs Springs made from heavily stabilized β titanium alloys are now commonly used in a large variety of shapes and sizes in airplanes. The prime reason is the low modulus of elasticity combined with the high yield stress. Titanium springs have two major advantages. First, they can save as much as 70 % in weight compared to steel springs; and second, they are immune to corrosion unlike steel springs. Details about the specific uses of the springs can be found in Ref. [13].

Flat springs are fabricated from strip, usually the alloy Ti-15-3. Springs made from round or square wire are commonly manufactured using the Beta C alloy. The processing route for the springs is the same as for β-annealed microstructures, which is normally used for heavily stabilized β alloys. If springs are required with a very low modulus of elasticity with reasonable strength, then the alloy is used without ageing. This is because ageing results in increasing the volume fraction of α phase, which in turn increases the modulus of elasticity.

Engine nacelles Another application worth mentioning is use of the heavily stabilized β alloy Beta 21S in the nacelle structure (exhaust plug, nozzle and aft cowl), e.g. Fig. 6.25, of the engines used for the Boeing 777 aircraft [13, 36].

Beta 21S sheets are used for this application because of the alloy's excellent oxidation resistance, which allows long-time operating temperatures in the range of 480–565 °C, with short-time periods up to 650 °C [53]. Beta 21S contains 15 %

Fig. 6.25 Use of Beta 21S as an engine tail plug (indicated by an *arrow*)

Mo and 2.7 % Nb, and was specially designed for high oxidation resistance. It also has excellent resistance to embrittlement when exposed to hydraulic fluid at elevated temperatures.

Beta 21S can be used for nacelle structures because the high temperature operational stresses are small. The Beta 21S sheets are basically used in the β-annealed condition, but two different final ageing treatments are used at Boeing [53]. These ageing treatments result in two different microstructures with quite different yield stress levels. Finally, it may be noted that a major European effort was initiated recently to use Beta 21S sheets in the exhaust structures of helicopter engines, in order to reduce the noise level of civil helicopters.

6.3 Summary

Conventional titanium alloys, especially near-α, α + β and the β alloys which have good strength and low densities, have a great future ahead. This is especially true in India, where many aircraft industries are being set up and the aerospace sector for repair and overhaul centres is growing. Because of this, the usage of titanium alloys can only grow, the only impediment being the cost.

Acknowledgments The authors wish to place on record that Prof G. Lütjering would certainly have been included as an author but for his untimely demise. Nevertheless, the authors cannot thank him enough for the repository of knowledge that he has created in the second edition of the book on Titanium, published by Springer publications. The authors would like to thank Dr. A.K. Gogia, Dr. T.K. Nandy and Mr. Dipak K. Gupta of DMRL; Mr. Ramesh Babu, Mr. G.V.R. Murthy and Mr. U.V. Gururaja of Midhani; and, Mr. V.P. Deep Kumar of ADA for many inputs and technical data. They profoundly thank the editors, Dr. N. Eswara Prasad and Dr. R.J.H. Wanhill for their help in reviewing the contents of the book chapter and also for their constructive comments. The authors (AB and BS) are greatly indebted to Prof D. Banerjee, Dr. K. Tamilmani, Dr. Samir V. Kamat and Dr. Amol A. Gokhale for their kind support and encouragement. Funding from DRDO is gratefully acknowledged.

References

1. Lütjering G, Williams JC (2007) Titanium: engineering materials and processes, 2nd edn. Springer, Berlin, Germany
2. Boyer R, Welsch G, Collings EW (eds) (1994) Materials properties handbook: titanium alloys. ASM International, Materials Park, OH, USA
3. Zarkades A, Larson FR (1970) Elasticity of titanium sheet alloys. In: Jaffee RI, Promisel NE (eds) The science, technology and application of titanium. Pergamon Press, Oxford, UK, pp 933–941
4. Conrad H, Doner M, de Meester B (1973) Deformation and fracture (controlling mechanisms for titanium plastic flow). In: Jaffee RI, Burte HM (eds) Titanium science and technology. Plenum Press, New York, USA, pp 969–1005

5. Partridge PG (1967) The crystallography and deformation modes of hexagonal close-packed metals. Metall Rev 12(1):169–194
6. Paton NE, Williams JC, Rauscher GP (1973) The deformation of alpha-phase titanium. In: Jaffe RI, Burte HM (eds) Titanium science and technology, Plenum Press, New York, USA, pp 1049–1069
7. Paton NE, Williams JC (1970) Second international conference on the strength of metals and alloys. ASM, Metals Park, OH, USA, p 108
8. Rosenberg HW, Jaffee RI (1970) The science, technology and application of titanium. In: Jaffee RI, Promisel NE (eds) Proceedings of the 2nd international conference on titanium, Pergamon Press, New York, USA, pp 851–859
9. Baker H (ed) (1992) Alloy phase diagrams, ASM handbook, vol 3. ASM, Materials Park, OH, USA
10. Newkirk JB, Geisler AH (1953) Crystallographic aspects of the beta to alpha transformation in titanium. Acta Metall 1(35):370, 373–371, 374
11. Williams JC (1973) Kinetics and phase transformations (in Ti alloys). In: Titanium science and technology, pp 1433–1494
12. Collings EW (1994) Materials properties handbook: titanium alloys. ASM, Materials Park, OH, USA
13. Boyer RR (1993) Applications of beta titanium alloys in airframes. In: Eylon D, Boyer RR, Koss Donald A (eds) Beta Titanium Alloys in the 1990's. The Minerals, Metal and Materials Society, Warrendale, PA, USA, pp 335–346
14. Buttrell WH, Shamblen CE (1999) Hearth melt plus vacuum arc remelt: production status. In: Titanium'95, science and technology, The Institute of Materials, London, UK, pp 1446–1453
15. Adams RT, Rosenberg HW (1982) Critical review a review of titanium ingot solidification. In: Williams JC, Belov AF Titanium and titanium alloys: scientific and technological aspects, 1st ed, Plenum Press, New York, USA, pp 127–135
16. Boyer R, Welsch G, Collings EW (eds) (1994) Materials properties handbook: titanium alloys, technical note 3: casting. ASM, Materials Park, OH, USA, pp 1079–1082
17. Eylon D, Froes FH, Gardiner RW (1983) Developments in titanium alloy casting technology. JOM 35(2):35–47
18. Schutz Ronald W, Thomas David E (1987) Corrosion of titanium and titanium alloys. In: ASM Handbook Nineth Edition, Volume 13 Corrosion, ASM, Metals Park, Ohio, USA, pp 669–706
19. Myers JR, Bomberger HB, Froes FH (1984) Corrosion behavior and use of titanium and its alloys. JOM 36(10):50–60
20. Schutz RW (1996) Development in Titanium alloy environmental behavior, titanium '95: science and technology. In: Proceedings of the eighth world conference on titanium. The Institute of Materials, London, UK, pp 1860–1870
21. Schutz RW (1994) Metallurgy and technology of practical titanium alloys. TMS, Warrendale, Pennsylvania, USA
22. Zwicker U (1974) Titan und Titanlegierungen. Springer-Verlag, Berlin, Germany, pp 102–107
23. Bania PJ, Parris WM (1990). Beta-21S: a high temperature metastable beta titanium alloy. In: Proceedings of the international conference on titanium products and applications, Titanium Development Association, vol 2, pp 784–793
24. Fleischer RL, Donald Peckner (1964) The strengthening of metals, vol 93. Reinhold, New York, USA
25. Okazaki K, Masuda I, Conrad H (1982) Mobile dislocation density during the plastic flow in Ti-interstitial alloys at low temperatures. In: Williams JC, Belov AF (eds) Titanium and titanium alloys: scientific and technological aspects, vol 1. Plenum Press, New York, USA, pp 497–505
26. Peters M, Lutjering G (1980) Control of microstructure and texture in Ti–6Al–4V. In: Jaffee RI, Kimura M, Izumi O (eds) Titanium '80, science and technology. AIME, Warrendale, PA, USA, pp 925–936

27. Lütjering G, Albrecht J, Ivasishin OM (1995) Influence of cooling rate and beta grain size on the tensile properties of (alpha + beta) Ti-alloys. In: Blenkinsop PA, Evans WJ, Flower HM (eds) Titanium '95: science and technology, vol 2. The Institute of Materials, London, UK, pp 1163–1170
28. Däubler MA, Helm D (1992) Surfaces and elevated temperature effects. In: Froes FH, Caplan IL (eds) Titanium '92: science and technology, vol 1. TMS, Warrendale, Pennsylvania, USA, pp 41–50
29. Ankem S, Seagle SR (1984) The detrimental effects of iron on creep of Ti-6242 S alloys. Titanium Sci Technol 4:2411–2418
30. Sinha V, Mills MJ, Williams JC (2001) Dwell-fatigue behavior of Ti-6Al-2Sn-4Zr-2Mo-0.1Si alloy. In: Jata K, Lee EW, Frazier W, Kim NJ (eds) Lightweight alloys for aerospace application. TMS, Warrendale, Pennsylvania, USA, pp 193–208
31. Woodfield AP, Gorman MD, Corderman RR, Sutliff JA, Yamrom B (1996) "Effect of microstructure on dwell fatigue behavior of Ti6242", titanium'95: science and technology. The Institute of Materials, Birmingham, UK, pp 1116–1123
32. Albrecht J, Lütjering G (2000) Microstructure and mechanical properties of titanium alloys. In: Gorynin IV, Ushkov SS (eds) Titanium '99: science and technology, vol 1. Central Research Institute of Structural Materials, St. Petersburg, Russia, pp 363–374
33. Peters JO, Lütjering G, Koren M, Puschnik H, Boyer RR (1996) Processing, microstructure and properties of β-CEZ. In: Blenkinsop PA, EvansWJ, Flower HM (eds) Titanium'95: science and technology, vol 2. The Institute of Materials, London, UK, pp 1403–1410
34. Sauer C, Busongo F, Lütjering G (2002) Fatigue 2002. EMAS, Warley, UK, pp 2043–2050
35. Bania PJ (1994) Beta titanium alloys and their role in the titanium industry. In: Vassel A, Eylon D, Combres Y (eds) Beta titanium alloys (Société Française de Métallurgie et de Matériaux, Paris, France), pp 7–15
36. Boyer RR (1994) Beta titanium alloys. Société Française de Métallurgie et de Matériaux, Paris, pp 253–261
37. Peters M, Lütjering G, Ziegler G (1983) Control of microstructures of α + β titanium alloys. Zeitschrift für Metallkunde 74:274–282
38. Köppers M, Herzig C, Freisel M, Mishia Y (1997) Intrinsic self-diffusion and substitutional Al diffusion in α-Ti. Acta Met 45:4181–4191
39. Helm D (1999) Application of titanium alloys as compressor discs and blades. In: Boyer RR, Eylon D, Lütjering G (eds) Fatigue behavior of titanium alloys. The Minerals, Metals and Materials Society, Warrendale, PA, USA, pp 291–298
40. Lütjering G, Helm D, Daubler M (1993)Influence of microstructure on fatigue properties of the new titanium alloy IMI 834. In: Bailon J-P, Dickson JI (eds) Fatigue 93 – Proceedings of the 5th international conference on fatigue and fatigue thresholds, vol 1. EMAS Publishing, Warrington, UK, pp 165–170
41. Thiehsen KE, Kassner ME, Pollard J, Hiatt DR, Bristow BM (1993) The effect of nickel, chromium and primary alpha phase on the creep behavior of Ti6242Si. Metall Trans 24A:1819–1826
42. Russo PA, Wood JR, Brosius RN, Marcinko SW, Giangiordano SR (1995) Influence of Ni and Fe on the creep of beta annealed Ti6242S. In: Blenkinsop PA, Evans WJ, Flower HM (eds) Titanium'95: science and technology, vol 2. The Institute of Materials, London, UK, pp 1075–1082
43. Russo PA, Yu KO (1999) Effect of Ni, Fe and primary alpha on the creep of alpha-beta processed and annealed Ti–6Al–2Sn–4Zr–2Mo–0.9Si. In: Gorynin IV, Ushkov SS (eds) Titanium'99: science and technology, vol 1. Central Research Institute of Structural Materials, St. Petersburg, Russia, pp 596–603
44. Ankem S, Seagle SR (1984) Heat-treatment of metastable beta titanium alloys. In: Boyer RR, Rosenberg HW (eds) Beta titanium alloys in the 1980's. TMS, Warrendale, Pennsylvania, USA, pp 107–126

45. Hayes RW, Viswanathan GB, Mills MJ (2002) Creep behavior of Ti–6Al–2Sn–4Zr–2Mo: I. The effect of nickel on creep deformation and microstructure Acta Mater, vol 50, pp 4953–4963
46. Viswanathan GB, Karthikeyan S, Hayes RW, Mills MJ (2002) Creep behaviour of Ti–6Al–2Sn–4Zr–2Mo: II. Mechanisms of deformation Acta Mater, vol 50, pp 4965–4980
47. Jeal RH (1982) Defects and their effect on the behaviour of gas turbine discs. In: 'Maintenance in service of high temperature parts', AGARD conference proceedings no. 317. Advisory Group for Aerospace Research and Development, Neuilly sur Seine, France, pp 6.1–6.15
48. Wagner L, Gregory JK (1993) Improvement of mechanical behavior in Ti–3Al–8V–6Cr-4Mo–4Zr by duplex aging. In: Eylon D, Boyer RR, Koss DA (eds) Beta titanium alloys in the 1990's. TMS, Warrendale, Pennsylvania, USA, pp 199–209
49. Prandi B, Wadier J-F, Schwartz F, Mosser P-E, Vassel A (1990) Titanium 1990, products and applications. Titanium Development Association (TDA) Dayton, Ohio, USA, pp 150–159
50. Peters JO, Lütjering G, Koren M, Puschnik H, Boyer RR (1996) Processing, microstructure, and properties of β-CEZ. Mater Sci Eng A 213(1):71–80
51. Combres Y, Champin B (1993) β-CEZ properties. In: Eylon D, Boyer RR, Koss Donald A (eds) Beta titanium alloys in the 1990's. TMS, Warrendale, PA, USA, pp 477–484
52. Peters M, Lütjering G (1976) Influence of grain-size on tensile properties of a Ti–Mo alloy with precipitate-free zones. Zeitschrift für Metallkunde 67:811–814
53. Boyer RR (1996) An overview on the use of titanium in the aerospace industry. Mater Sci Eng A 213(1):103–114

Bibliography

1. Leyens C, Peters M (eds) (2003) Titanium and titanium alloys: fundamentals and applications. WILEY VCH Verlag GmbH & Co. KGaA, Weinheim, Germany